JOURNAL OF MATERIALS SCIENCE 26 (1991) 1666–1672

Contribution to the study of SnO_2-based ceramics

Part I *High-temperature interactions of tin(IV)oxide with antimony(III)oxide and copper(II)oxide*

M. ZAHARESCU, S. MIHAIU, S. ZUCA
Centre of Physical Chemistry, Romanian Academy, Bucharest, Romania
K. MATIASOVSKY
Institute of Inorganic Chemistry, Centre for Chemical Research, Slovak Academy of Sciences, Bratislava, Czechoslovakia

Sintered SnO_2-based ceramics are considered to be promising construction materials for manufacturing stable electrodes for various technological applications. The high-temperature interactions of components, important with respect to the sintering capacity and consequently the densification, have been investigated in the binary systems SnO_2–Sb_2O_3 and SnO_2–CuO, and the ternary system SnO_2–Sb_2O_3–CuO. In contrast to the SnO_2–Sb_2O_3 mixtures with a poor sintering ability, the binary SnO_2–CuO and ternary SnO_2–Sb_2O_3–CuO mixtures exhibit significantly improved sintering properties owing to the formation of liquid phase (eutectic melt) in the presence of copper(II)oxide.

1. Introduction

Tin(IV)oxide-based ceramic materials are considered to be very interesting with respect to their application potential in the manufacturing of stable electrodes, namely for aluminium electrolysis (inert anodes [1]) and the glass industry [2, 3]. For this purpose, a high electrical conductivity and high sintering ability of the substrate powder ensuring a high density and, consequently low porosity of the final product are imperative. Addition of various metallic oxides has been suggested to increase the electrical conductivity and raise the sintering capacity of SnO_2 [4]. The best results were claimed for a combined addition of Sb_2O_3 and CuO [5–8]. The addition of antimony(III)oxide is claimed to increase dramatically (by four to five orders of magnitude) the electrical conductivity of SnO_2 which is attributed to the increased charge carrier concentration [9, 10]. Copper(II)oxide is added in order to improve the sintering ability and enhance the densification of SnO_2.

The data on the interactions of SnO_2 with Sb_2O_3 and/or CuO which might be of prime importance for establishing the optimum composition of the SnO_2-based composite are rather scarce. Actually, except for the information on the limited solid solubility of Sb_2O_3 (up to 20 to 25% at 1000 °C) in SnO_2 [11, 12] there are virtually no data on the high-temperature interactions in the binary system SnO_2–Sb_2O_3 and SnO_2–CuO, and in the ternary system SnO_2–Sb_2O_3–CuO. This investigation has been performed in the present study. The binary systems were investigated within the whole composition range and the ternary system in the SnO_2-rich (over 90%) region.

2. Experimental details

The samples were composed from SnO_2, Sb_2O_3, CuO all reagent grade. Their thermal and structural properties are listed in Table I. Mixtures of oxide powders (grain size below 60 μm) were homogenized in acetone.

The interactions between the components in the studied systems were investigated in both isothermal and non-isothermal conditions.

The non-isothermal measurements were carried out by differential thermal analysis (DTA) and thermogravimetry (TG) up to 1200 °C at a heating rate of 7.5 °C min^{-1} using a MOM OD-103 Derivatograph.

The isothermal study was performed at temperatures from 600 to 1200 °C. Cylindrical samples obtained by pressing at 30 MPa were kept at the given temperature for 1 h and then quenched in the atmosphere.

After thermal treatment, the samples were analysed by X-ray diffractometer using a TUR M-62 apparatus equipped with a HZG-3 diffractometer operating with CuKα radiation. The porosity was determined by weighing samples before and after 24 h immersion in toluene. The linear shrinkage was determined by measuring the diameter of samples before and after thermal treatment.

0022–2461/91 $03.00 + .12

TABLE I Structural and thermal properties of components

Oxide	Crystallographic system	Lattice parameters (nm)	Thermal behaviour	References
SnO_2	tetragonal	$a_0 = 0.4738$ $c_0 = 0.3188$	no changes	[13, 14]
CuO	monoclinic	$a_0 = 0.4684$ $b_0 = 0.3425$ $c_0 = 0.5129$	$CuO \xrightarrow{1075\,°C} Cu_2O$	[13–15]
Sb_2O_3	orthorhombic	$a_0 = 0.4914$ $b_0 = 1.2468$ $c_0 = 0.5421$	$Sb_2O_3 \longrightarrow Sb_2O_4$	[13–15]
Sb_2O_3	cubic	$a_0 = 1.1152$	$Sb_2O_3 \longrightarrow Sb_2O_4$	[13–15]
Sb_2O_4	orthorhombic	$a_0 = 0.5436$ $b_0 = 0.4810$ $c_0 = 1.176$		[13, 14]

3. Results and discussion

3.1. Non-isothermal measurements

Experimental data determined under non-isothermal conditions for pure components and selected binary and ternary mixtures are listed in Table II.

It can be seen that in the case of pure components the results of the DTA and TG measurements are consistent with the literature data (see Table I). The endothermal reduction of CuO to Cu_2O which starts at 1075 °C and is accompanied by a mass loss, is followed by eutectic melting of the two copper oxides. On the other hand, the oxidation of Sb_2O_3 to Sb_2O_4, which takes place within a wide temperature interval from 440 to 660 °C, is accompanied by a well marked exothermal effect and a mass increase. The endothermal effect observed at 1160 °C indicates the vaporization of Sb_2O_4.

The temperature interval of the exothermal effect corresponding to the oxidation of Sb_2O_3 is substantially narrowed in the binary and ternary mixtures which suggest the catalysing effect of SnO_2 in the oxidation process. It may be also assumed that in the reaction with SnO_2 antimony participates as a heterovalent mixture of the Sb(III)Sb(V)O_4 type. The endothermal effect observed at high Sb_2O_3 concentrations at temperatures above 1150 °C, which is accompanied by a mass loss, is ascribed to the vaporization of Sb_2O_4.

3.2. Isothermal measurements

The composition and the main properties (shrinkage, porosity and phase composition) of the thermal treated samples are listed in Tables III to V. The temper-

TABLE II The results of differential thermal analyses and thermogravimetry of samples of the SnO_2–Sb_2O_3–CuO system

Sample	Thermal effects		Mass variation		Assignment
	Endo (°C)	Exo (°C)	Experiment (%)	Calculated (%)	
SnO_2	No effects				
Sb_2O_3		440–660	+ 5.1	+ 5.5	$Sb_2O_3 \rightarrow Sb_2O_4$
	1160				Sb_2O_4 vaporization
CuO	122		− 2.0		Water evolution
	1075		− 9.6	− 10.1	$CuO \rightarrow Cu_2O$
	1080				Eutectic melting
94% SnO_2 + 6% Sb_2O_3		422–465	+ 0.25	+ 0.33	$Sb_2O_3 \rightarrow Sb_2O_4$
80% SnO_2 + 20% Sb_2O_3		440	+ 0.87	+ 1.10	$Sb_2O_3 \rightarrow Sb_2O_4$
	1155				Sb_2O_4 vaporization
70% SnO_2 + 30% Sb_2O_3		443	+ 1.36	+ 1.64	$Sb_2O_3 \rightarrow Sb_2O_4$
	1163				Sb_2O_4 vaporization
20% SnO_2 + 80% CuO	1060		+ 7.10	+ 8.00	$CuO \rightarrow Cu_2O$ and eutectic melting
10% SnO_2 + 90% CuO	1060		+ 7.80	+ 9.00	$CuO \rightarrow Cu_2O$ and eutectic melting
92% SnO_2 + 2% CuO + 6% Sb_2O_3		420–455	+ 0.34	+ 0.33	$Sb_2O_3 \rightarrow Sb_2O_4$

TABLE III Sintering properties and phase composition of samples in the system SnO_2–Sb_2O_3

	Composition		Thermal treatment, 1 h											
	SnO_2 (%)	Sb_2O_3 (%)	600 °C			800 °C			1000 °C			1200 °C		
			Shrinkage (%)	Porosity (%)	Phase composition	Shrinkage (%)	Porosity (%)	Phase composition	Shrinkage (%)	Porosity (%)	Phase composition	Shrinkage (%)	Porosity (%)	Phase composition
1	100	0	0	10.8	SnO_2	0.2	10.6	SnO_2	0.2	8.1	SnO_2	0.7	9.1	SnO_2
2	98	2	0.7	10.6	SnO_2	0.7	10.5	SnO_2	0.1	8.5	SnO_2	0	8.8	SnO_2
3	96	4	0.4	10.1	SnO_2	0.4	10.1	SnO_2	0.2	8.9	SnO_2	0	8.7	SnO_2
4	94	6	0.7	10.0	SnO_2	0.7	10.0	SnO_2	0.1	9.0	SnO_2	0	8.9	SnO_2
5	92	8	0	9.8	SnO_2	0	9.6	SnO_2	0.2	9.5	SnO_2	0	7.7	SnO_2
6	90	10	0.6	10.1	SnO_2	0.6	9.1	SnO_2	0.1	10.9	SnO_2	0.1	7.6	SnO_2
7	80	20	0.4	9.6	SnO_2, Sb_2O_4	0	8.2	SnO_2, Sb_2O_4	0	8.9	SnO_2			
8	70	30	0.3	8.5	SnO_2, Sb_2O_4	0	3.4	SnO_2, Sb_2O_4	0.3	8.8	SnO_2			
9	60	40	0.2	10.0	SnO_2, Sb_2O_4	0	4.0	SnO_2, Sb_2O_4	0					
10	50	50	0	9.4	SnO_2, Sb_2O_4									
11	40	60	0	10.0	SnO_2, Sb_2O_4									
12	30	70	0	8.9	SnO_2, Sb_2O_4									
13	20	80	0	10.8	SnO_2, Sb_2O_4									
14	10	90	0	13.6	SnO_2, Sb_2O_4									
15	0	100	0	9.1	Sb_2O_4									

Deformed samples

Deformed samples

Deformed samples

TABLE IV Sintering properties and phase composition of masses in the system SnO_2–CuO

	Composition		Thermal treatment, 1 h								
	SnO_2 (%)	CuO (%)	900 °C			1000 °C			1200 °C		
			Shrinkage (%)	Porosity (%)	Phase composition	Shrinkage (%)	Porosity (%)	Phase composition	Shrinkage (%)	Porosity (%)	Phase composition
1	100	0	0	5.1	SnO_2	0.1	4.7	SnO_2	0.7	9.1	SnO_2
2	99	1	7.7	3.1	SnO_2	9.1	1.0	SnO_2	6.8	0	SnO_2
3	98	2	5.5		SnO_2	10.4		SnO_2	12.6	0	SnO_2
4	96	4	5.2		SnO_2	11.2		SnO_2	12.0	0	SnO_2
5	95	5	5.8		SnO_2	11.9	1.0	SnO_2	12.2	0	SnO_2
6	94	6	5.9		SnO_2	10.0		SnO_2	11.1	0	SnO_2
7	92	8	5.8		SnO_2	10.8		SnO_2	10.9	0	SnO_2
8	90	10	5.7	2.4	SnO_2, CuO	10.4	0	SnO_2, Cu_2O	9.7	0	SnO_2
9	80	20	4.4	2.7	SnO_2, CuO	9.7	0	SnO_2, Cu_2O			
10	70	30	4.7	2.8	SnO_2, CuO	9.7	0	SnO_2, Cu_2O, CuO			
11	60	40	4.5	2.8	SnO_2, CuO	9.0	0	SnO_2, Cu_2O, CuO			
12	50	50	4.6	2.9	SnO_2, CuO	9.3	0	SnO_2, Cu_2O, CuO			
13	40	60	4.4	3.0	SnO_2, CuO	9.6	0	SnO_2, Cu_2O, CuO			
14	30	70	4.5	2.5	SnO_2, CuO	12.4	0	SnO_2, Cu_2O, CuO			
15	20	80	4.9	4.0	SnO_2, CuO	13.6	0	SnO_2, Cu_2O, CuO			
16	10	90	4.7	4.0	SnO_2, CuO	11.5	0	SnO_2, Cu_2O, CuO			
17	0	100	2.0	4.7	CuO	13.5	0	Cu_2O, CuO			

the samples melt

TABLE V Sintering properties and phase composition of samples in the system SnO_2–Sb_2O_3–CuO

	Composition			Thermal treatment, 1 h								
				900 °C			1000 °C			1200 °C		
	SnO_2 (%)	CuO (%)	Sb_2O_3 (%)	Shrinkage (%)	Porosity (%)	Phase composition	Shrinkage (%)	Porosity (%)	Phase composition	Shrinkage (%)	Porosity (%)	Phase composition
1	96	2	2	2.5	5.0	SnO_2	2.9	4.8	SnO_2	11.3	0	SnO_2
2	94	2	4	1.3	5.3	SnO_2	0.7	5.2	SnO_2	11.2	0	SnO_2
3	94	4	2	2.9	4.9	SnO_2	3.1	4.4	SnO_2	10.6	0.3	SnO_2
4	92	2	6	0.6	5.1	SnO_2	0.6	4.9	SnO_2	10.9	0.1	SnO_2
5	92	4	4	1.3	5.4	SnO_2	2.0	5.0	SnO_2	9.6	0.4	SnO_2
6	92	6	2	3.4	4.6	SnO_2	4.0	4.1	SnO_2	10.1	0.3	SnO_2
7	90	2	8	0.5	5.2	SnO_2	0.9	4.9	SnO_2	9.1	0.5	SnO_2
8	90	4	6	1.3	5.5	SnO_2	1.6	5.3	SnO_2	9.7	0.4	SnO_2
9	90	6	4	2.3	5.1	SnO_2	3.5	4.9	SnO_2	9.8	0.3	SnO_2
10	90	8	2	3.7	5.0	SnO_2	3.7	4.3	SnO_2	9.8	0.3	SnO_2

atures of the thermal treatment were selected taking into account the phase transformation temperatures of components.

Table III shows the experimental results for the SnO_2–Sb_2O_3 system. The exothermal effect indicates the oxidation of Sb_2O_3 to Sb_2O_4 at 600 °C, however, the latter oxide has not been identified by X-ray diffraction at concentrations up to 10% (all concentrations are given in mass %). This can be apparently assigned to the formation of the solid solution owing to the substitution of antimony for tin in the SnO_2 crystal structure. Although the samples with a higher Sb_2O_4 concentration undergo deformation and peeling at higher temperatures which make them unsuited for the subsequent measurements, the concentration of Sb_2O_4 in the solid solution apparently increases with increasing temperature and only SnO_2 is identified in the undeformed samples. This is evident in Fig. 1 for a mixture containing 30% Sb_2O_3: the intensity of diffraction peaks characteristic for SnO_2 increases with increasing temperature while the intensity of diffraction peaks characteristic for Sb_2O_4 decreases to zero at 1000 °C. The low linear shrinkage and high porosity indicate the inadequate sintering of the samples.

The experimental data on the binary SnO_2–CuO system are shown in Table IV. Here again the diffraction peaks characteristic for copper(II)oxide only were observed at higher CuO contents (from 10% onwards). In contrast to Sb_2O_3, however, copper does

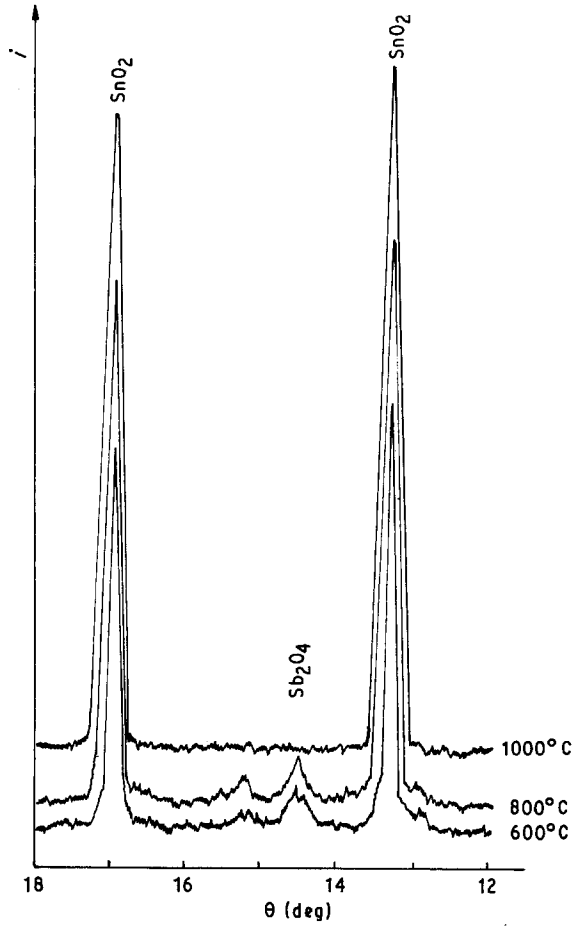

Figure 1 Part of a diffraction diagram indicating the inclusion of Sb_2O_4 in SnO_2 structure at different temperatures (70% SnO_2 + 30% Sb_2O_3 mixture).

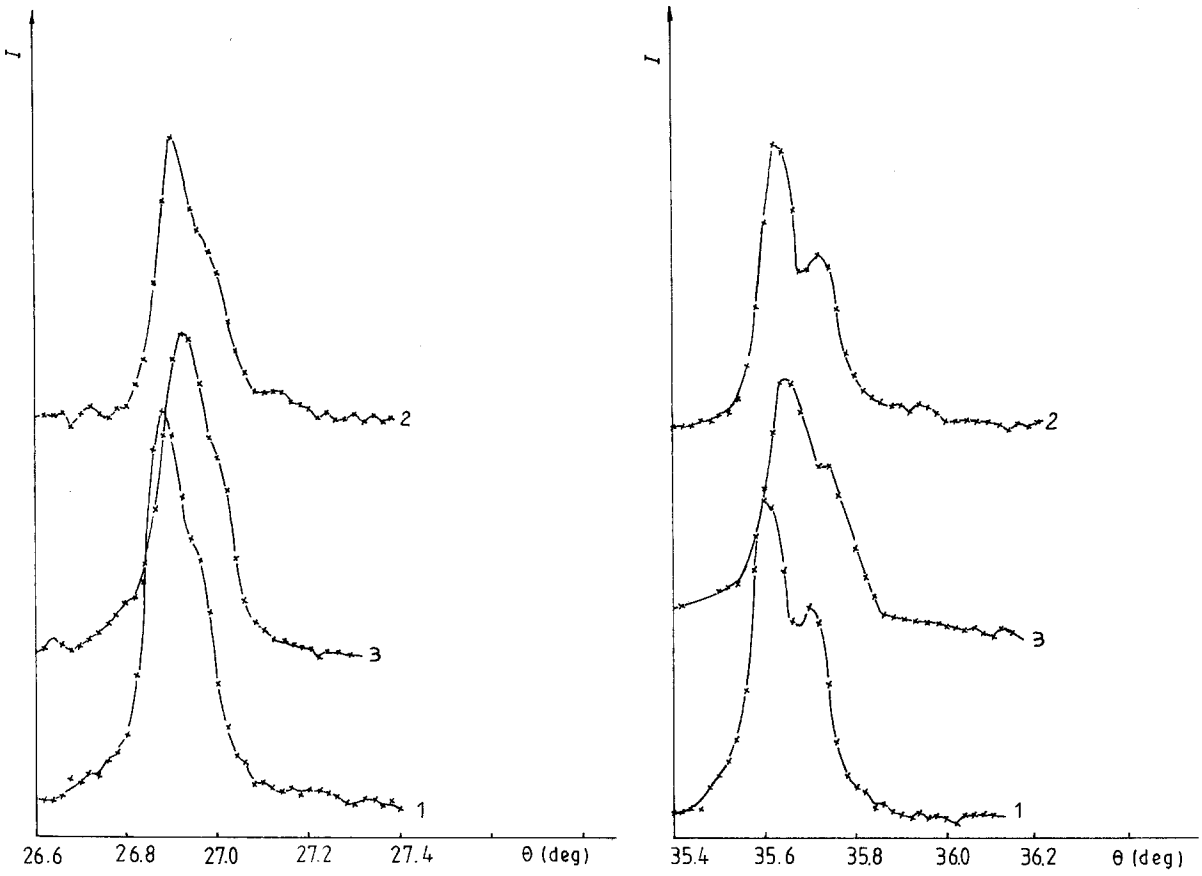

Figure 2 Shifts of the maxima in parts of diffraction diagrams indicating the variations of the SnO_2 lattice parameters in samples thermally treated at 1200 °C. (1, SnO_2, 2, 96% SnO_2 + 4% Sb_2O_3, 3, 92% SnO_2 + 6% Sb_2O_3 + 2% CuO)

not enter into the crystal structure of SnO_2 and the absence of the diffraction peaks corresponding to CuO was interpreted by its penetration into the liquid phase (eutectic melt). At higher contents, CuO is identified in amounts proportional to initial concentrations which indicates that the two oxides do not interact in the solid state.

As seen in Table IV, the reduction of CuO to Cu_2O in isothermal conditions takes place at substantially lower temperature compared with the non-isothermal measurements. At 1000 °C, the process proceeded almost quantitatively and only low contents of unreduced CuO were identified in samples with a high initial concentration ($\geqslant$ 30% of copper(II)oxide).

The samples with a CuO content exceeding 10% fused when thermally treated at 1200 °C. In those with a lower concentration of CuO only the presence of SnO_2 has been identified which indicated the onset of the eutectic melting.

The shrinkage of the tested samples increased with increasing temperature while the porosity decreased; at 1000 and 1200 °C samples with a zero porosity were obtained, apparently owing to the presence of the liquid phase.

The experimental data on the SnO_2–CuO system indicate that no permanent binary compounds are formed under the given experimental conditions.

The results obtained in the study of the SnO_2-rich region of the ternary system SnO_2–Sb_2O_3–CuO are listed in Table V. SnO_2 was the only phase component identified in the samples following the thermal treatment at all temperatures which suggest a partial substitution of antimony for tin in the SnO_2 crystal structure and the accumulation of CuO(Cu_2O) in the eutectic melt. The substitution of antimony for tin is evinced by the variation of the lattice parameters of SnO_2 shown in Fig. 2 and Table VI.

TABLE VI Variations of SnO_2 lattice parameters in samples thermally treated at 1200 °C

	Sample	Lattice parameter	
		a_0 (nm)	c_0 (nm)
1	SnO_2	0.4739 (7)	0.3189 (6)
2	96% SnO_2 + 4% Sb_2O_3	0.4739 (7)	0.3187 (4)
3	92% SnO_2 + 2% CuO + 6% Sb_2O_3	0.4732 (4)	0.3185 (4)

The determined values for the linear shrinkage and porosity evince a high densification of samples, namely those thermally treated at 1200 °C, although the beneficial effect of CuO on sintering of SnO_2 and Sb_2O_3 becomes evident even at lower temperatures as it follows from a comparison of the experimental data in Tables III and V.

The affect of additions of various oxides on the electrical conductivity of SnO_2-based ceramic materials will be discussed in the subsequent paper.

4. Conclusions

Based on experimental data and the preceding discussion, the following conclusions can be drawn on the

high-temperature interactions of SnO_2, Sb_2O_3, and CuO.

(1) The phase analysis of the thermally treated samples of the system SnO_2–Sb_2O_3 has confirmed the literature data on a limited solid solubility of Sb_2O_3 in SnO_2. The solubility increases with increasing temperature. The samples exhibit a poor sintering ability.

(2) Eutectic melt is formed in the system SnO_2–CuO. The presence of a liquid phase above 900 °C significantly improves sintering and densification.

(3) SnO_2-based solid solutions only were identified in the system SnO_2–Sb_2O_3–CuO over the whole concentration range investigated (SnO_2 contents above 90%). The improved sintering properties and, consequently a higher densification in the ternary system compared with those determined in the system SnO_2–Sb_2O_3 are ascribed to the formation of the eutectic melt in the presence of CuO.

Acknowledgements

Thanks are extended to Mrs V. Leahu from Centre of Physical Chemistry, Bucharest, Romania, for help in running X-ray measurements and to Dr V. Figusch and Dr M. Haviar from the Institute of Inorganic Chemistry, Centre for Chemical Research, Slovak Academy of Sciences, Bratislava, Czechoslovakia, for performing parallel dilatometric measurements of selected samples.

References

1. K. BILLEHAUG and H. A. ØYE, *Aluminium* **57** (1981) 146.
2. W. ZIEMBA and B. ZIEMBA, *Szklo i Ceram.* **24** (1973) 12.
3. T. CHVATAL, *Sprechsaal Keram. Glass Baust.* **B107** (1974) 1057.
4. H. ALDER, US Patent 4057480 (1977).
5. *Idem*, US Patent 3930967 (1976).
6. *Idem*, US Patent 3960678 (1976).
7. J. M. CLARK and D. R. SECRIST, *US Patent* 4379033 (1983).
8. D. R. SECRIST and J. M. CLARK, US Patent 4448997 (1984).
9. L. D. LOCH, *J. Electrochem. Soc.* **110** (1963) 108.
10. R. W. MAR, *J. Phys. Chem. Solids* **33** (1972) 220.
11. E. V. DEGTYAREVA, B. G. ALAPIN, V. J. DROZD, I. I. KABAKOVA, S. V. LYSAK and N. V. GULKO, *Ogneupory* **10** (1978) 40.
12. B. G. ALAPIN, E. U. DEGTYAREVA, V. J. DROZD, N. V. GULKO and S. V. LYSAK, *Izv. Akad. Nauk SSSR, Neorg. Mat.* **17** (1981) 923.
13. C. PASCAL, *Nouveau traité de chimie mineral*, Vol. 4, 8 (Masson et Cie., Paris, 1958, 1963).
14. JCPDS Powder Diffraction File: 19081 (1973).
15. E. M. LEVIN, C. R. ROBBINS and H. F. McMURDIE, "Phase Diagrams for Ceramists" (The American Ceramic Society, Columbus, Ohio, 1964) (Supplement 1969).

Received 5 May
and accepted 17 October 1989